Metal Flow Through a Filter System

A Habibollah Zadeh, J Campbell
IRC in Materials Processing
School of Engineering
University of Birmingham, Edgbaston, Birmingham, England

ABSTRACT

The flow of Al-Si alloy and cast iron liquids inside a filtering system comprised of a bubble trap and a tangentially oriented 20-ppi ceramic foam filter has been investigated by the use of video x-ray radiography. Comparison of experimental and simulation results confirms that there is a laminar, viscosity dependant flow in the filter. Outside the filter, the narrow channels used in this study favoured a laminar flow regime, although normally a turbulent inertially dependant flow outside the filter would apply in most conventional systems in which the running system is expanded around the filter. The total effect for the complete system is a mixed flow regime. Comparing the experiments with three different computer simulation models revealed that all the models were impressively good. The differences between the predictions of the models appeared to be mainly the result of the choice of physical input data. It was revealed that the liquid metal could partially solidify inside the filter depending on the volume per cent of porosity and ratio of surface area to volume of the filter.

INTRODUCTION

Investigations (1-3) have shown two main effects of filters (i) reducing of inclusions in the poured metal by simple filtration, and (ii) controlling the flow so as to reduce the re-introduction of inclusions downstream of the filter. Hence, filters are being widely accepted as a standard tool of good casting practice. There are different kinds of filters such as woven glass cloth, steel wire mesh, and ceramic filters that are extruded, pressed or foam types.

When designing a filling system for a casting, it has become a problem to know how to allow for the presence of the filter in the system. Clearly, it introduces drag, reducing the flow rate. Experimental attempts to assess this effect have employed air or water to measure the flow properties through the filter. Additional approaches have employed purely mathematical computation (4-5). In principle, the pressure drop data for the filter system is useful for predicting the liquid behaviour and outlet velocity from the filter system in practical situations, allowing the outlet velocity to be estimated and an appropriate gating system to be designed.

In our recent studies of the filling of tall, thin section castings, the flow of high velocity liquid metal has been investigated. In this application the filtering system consisted of a filter inlet, a bubble trap, a ceramic foam filter and a filter outlet. The bubble trap is a cavity designed to provide an alternative path for the bubbles, and other low density material such as dross or slag, diverting these materials from accumulating at the filter and finally being forced through, entering the casting. It can only do this if it is designed for the first melt, which may be cool or contaminated with debris, to be diverted into and retained in the trap. One particular design of filtering system, comprising all of these features, is used here. The design has been demonstrated to achieve calm and clean liquid, resulting sound castings of aluminium alloys and cast iron. The details of the design have been described elsewhere. (6,7)

In this paper, the detailed flow behaviour of the liquid metal in such a filtering system has been modelled in three computer simulations. The predictions are described and compared with the experimental results.

EXPERIMENTAL PROCEDURE

Figure 1 show a schematic illustration of the casting geometry used in the first experiment. In second test a filtering system was incorporated in the main channel (Figure 2). The moulds were made from silica and bonded with a phenolic urethane based resin (Ashland Pepset). The liquid metals were Al-12.5%Si alloy and cast iron with nominal composition of 3.4%C, 2.5%Si, 0.56%Mn, 0.06%S (CE ≡ 4.23).

The assembled mould was placed in real-time x-ray radiographic unit so that the filling sequence of casting during priming of the liquid metal could be recorded on video tape at 50 frames per second. These data made it possible to measure the velocity of the melt entering the casting (in this case the casting simply consisting of the straight channel of the fluidity mould) with and without the filtering system (Table 1). Also, the geometry and time of flow in the filtering system were determined.

SIMULATION METHODS

Two computer codes (Magmasoft and FLOW3D) were employed to simulate the fluid flow and solidification of liquid metal in a channel with and without a filtering system. The Navier-Stokes equation and K-ε turbulent model were adopted to perform numerical calculations and used in all subsequent simulation of fluid flow (8,9).

The Filter Models

Three models for simulating of the filter were employed to compare the results with experiments:

(1) In first model (8), the equation to describe the pressure drop across the filter is:

$$\Delta P = K_1 U + K_2 U^2 \qquad \text{Equation 1}$$

Where U is velocity of liquid metal and constants K_1, K_2 are coefficients for laminar and turbulent flow, which require to be experimentally determined. Using the database provided in the software, for a 20 ppi filter K_1 is zero (i.e. effectively assumes no Darcy type laminar flow contribution) and K_2 is 138122 kg/m^3 in all-possible directions of flow. Thus the rather general Equation 1 is effectively reduced to merely a turbulent flow model by the assumption of $K_1 = 0$.

2) In second filter model (9), the filter is represented by a drag coefficient (K) on the fluid in the filter volume, assuming Darcian flow. Thus the pressure drop (ΔP) is linearly dependent upon the velocity (U);

$$\Delta P = \rho \Delta x K U \qquad \text{Equation 2}$$

Where $K(= AV_F^{-B})$ is the drag coefficient and is dependent on the filter porosity (V_F), thickness of filter (Δx) and liquid density (ρ). Thus the pressure drop approximates to:

$$\Delta P = aV_F^{-B} U \qquad \text{Equation 3}$$

Where $a = A(\rho \Delta x)$, and A and B are empirically defined constants. The following measured parameters were adopted from work of Lo (5)

A = 29.33 b = 7.37 V_F = 0.753

3) For high flow velocity, Forchheimer (10) has suggested the modification of Darcy's law by the intoduction of a quadratic velocity term to take into account the increasing influence of the inertial force due to liquid high velocity. His Forchheimer-extended Darcy model is:

$$\frac{\Delta P}{L} = \frac{\mu}{k} U + \frac{\rho C_F}{k^{0.5}} U^2 \qquad \text{Equation 4}$$

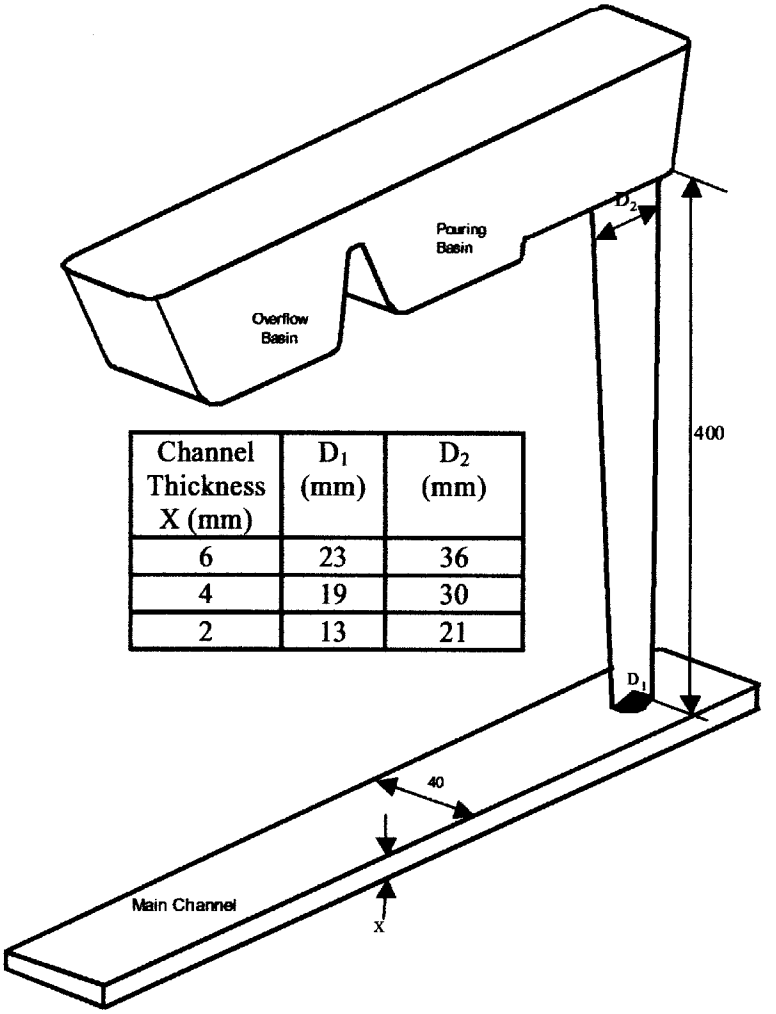

Channel Thickness X (mm)	D_1 (mm)	D_2 (mm)
6	23	36
4	19	30
2	13	21

Figure 1: schematic illustration of pouring basin, sprue and main channel (runner) prior to the addition of a filter (dimensions in millimetre).

Table 1: Results of velocity measurement of Al-Si alloy and cast iron liquids in different channel thicknesses by the use of real-time x-ray radiography technique.

	Liquid metal velocity (m/s)			
	Al-Si alloy		Cast iron	
Channel Thickness (mm)	Unfiltered	Filtered	Unfiltered	Filtered
2	1.95	0.36	1.88	0.39
4	2.76	0.58	2.85	0.58
6		0.615		0.765

a)

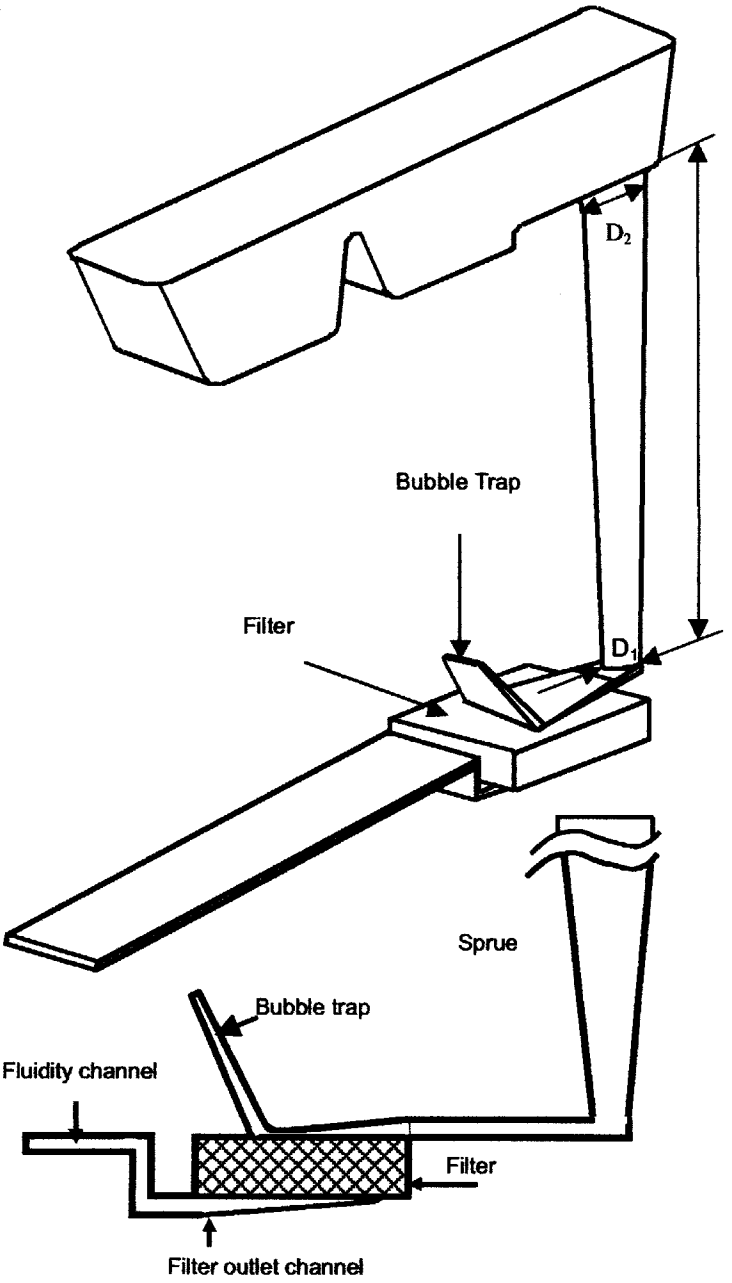

b)

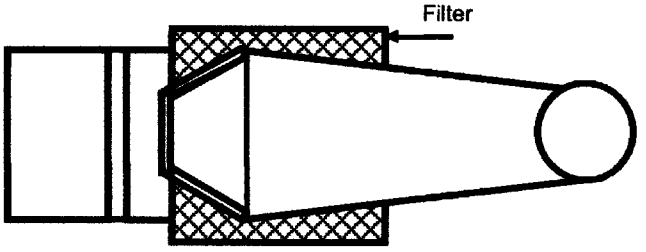

Figure 2: Schematic illustration of a) filtered fluidity test set up, and b) filter system (dimensions in millimetre).

where

ΔP = Pressure difference
L = Length of the filter, equivalent to □x,
k = permeability,
μ = viscosity, and
C_F = Inertia coefficient.

The equation is equivalent to Equation 1. To take into account the inertial effects of the flow inside of the filter, in this third filter model the drag coefficient K was calculated as (9)

$$K = \frac{\mu}{\rho}\frac{1-V_F}{V_F^2}\left\{a(1-V_F)+b\frac{R_e}{d}\right\} \qquad \text{Equation 5}$$

Where Re (=Udρ/μ) is the Reynolds number and d is the fiber diameter of the filter. The constants a and b in the Equation 4 are described as;

$$a = \frac{\alpha}{d^2}$$

$$b = \frac{\beta}{d}$$

where d = fibre diameter of the filter (m). In this filter model we needed to experimentally determine the fiber size of the filter. Measuring of 100 fiber diameters (d in Equation 4) in five filters in both the surface and depth of the filters revealed the average fiber diameter of a 20 ppi filter to be about 0.4 mm. (Note by the authors: the choice of fibre diameter of the filter seems somewhat perverse. This would be more appropriate to the situation where flow is through a fibre mesh, as in the impregnation of a ceramic fibre preform. For a foam filter it would surely be more appropriate for the formula to be presented in terms of the average pore diameter, so that the representative length would be most appropriately the hydraulic radius, i.e. half the average radius, of the pores)

According to the FLOW3D manual (9) α is 180 and β is a surface roughness which was selected to be 4.0. To assess the effect of filter porosity, three values, 92, 75 and 55% were chosen for V_F. The values of 92 and 75% were adopted from two different references (4, 5), that have suggested these porosity values for a 20 ppi filter.

RESULTS

Figures 3 and 4 show the recorded results of video x-ray radiography from the filling sequence of the filtering system. The results of velocity measurements of Al-Si alloy and cast iron liquids (Table 1) are plotted in Figures 5 and 6, respectively.

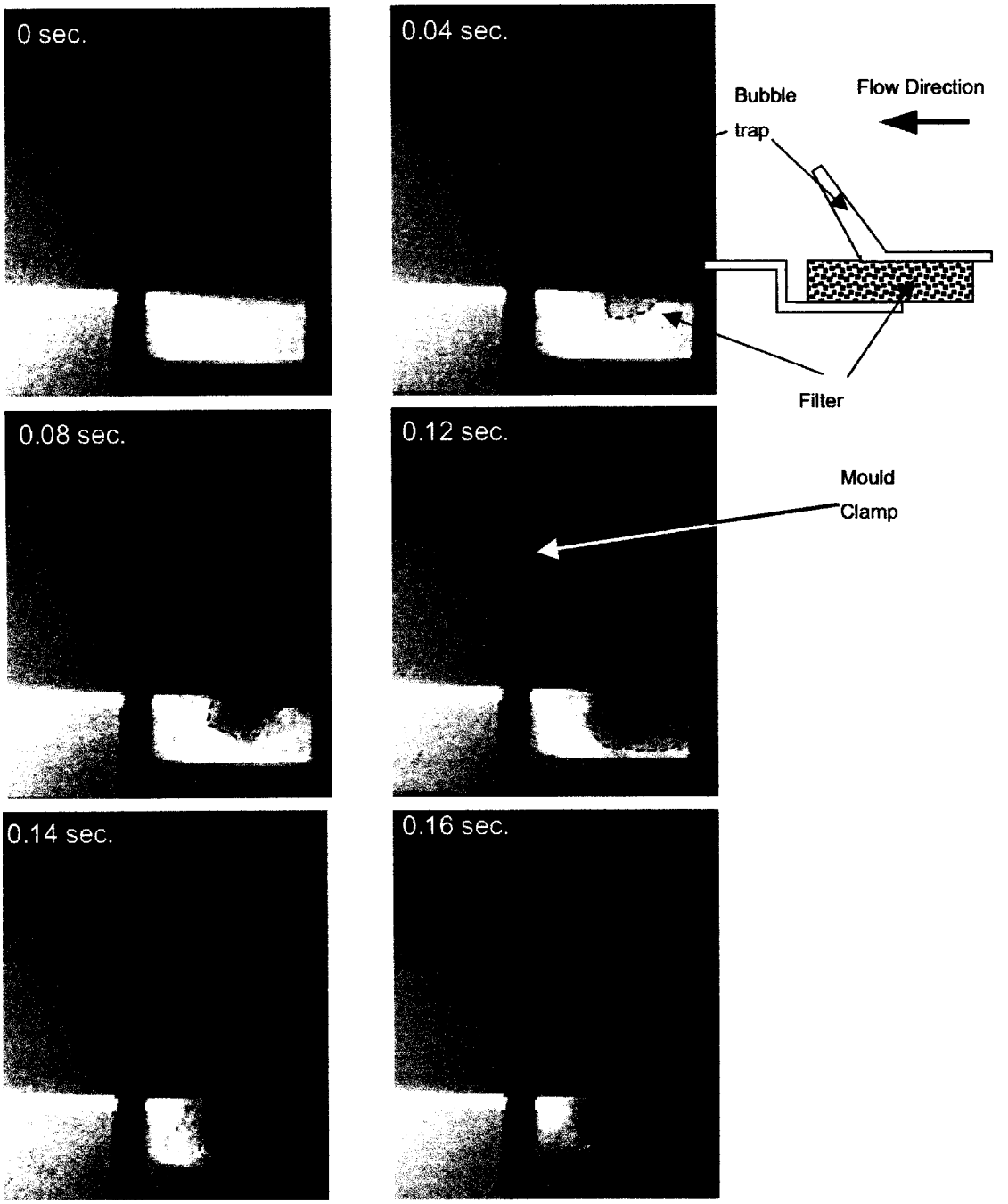

Figure 3: Flowing sequence of Al-13%Si melt in a ceramic foam filter, using design as in Figure 2. Channel thickness is 4 mm. Dot lines roughly show the liquid front in each frame.

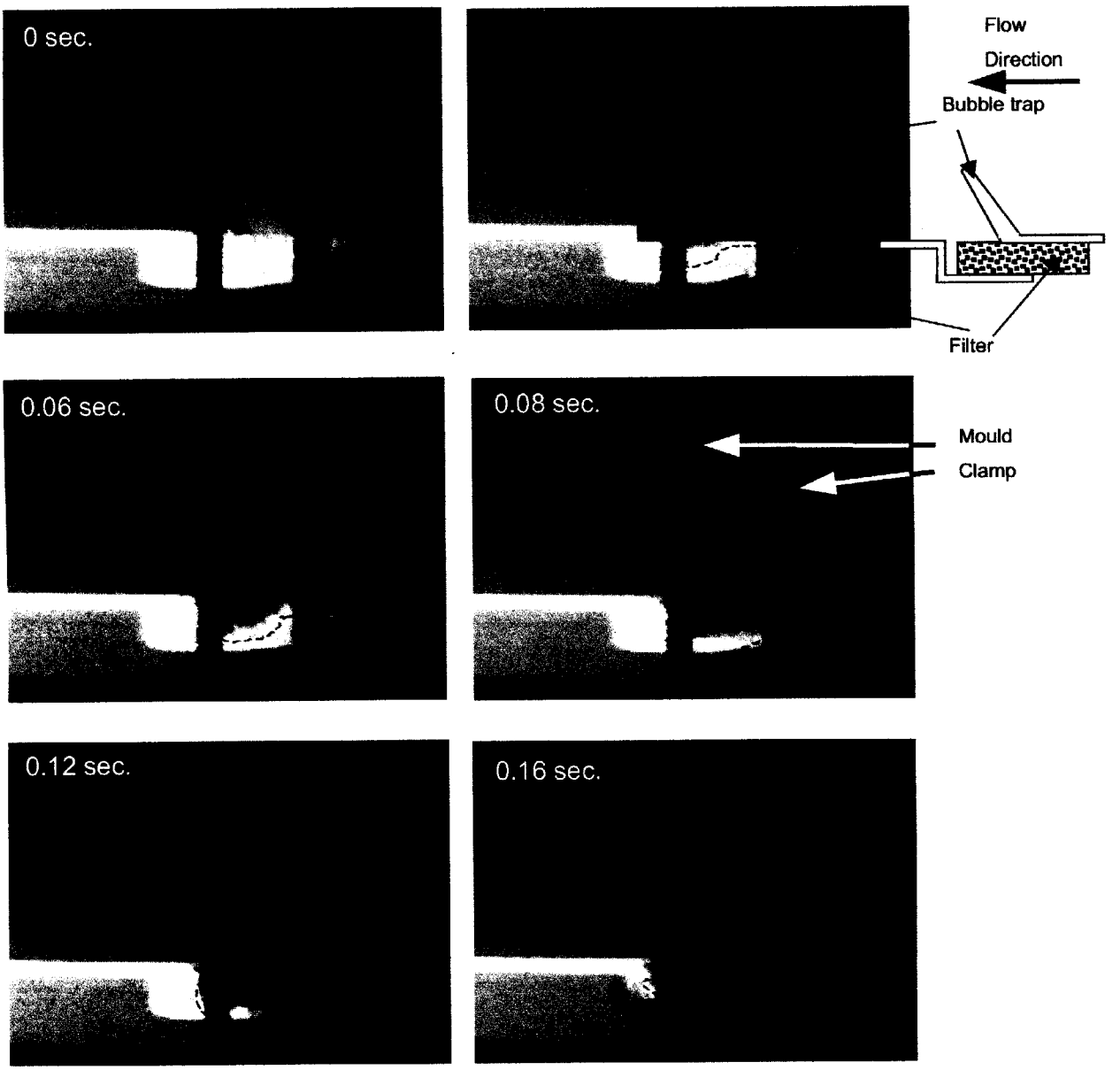

Figure 4: Flowing sequence of cast iron melt at 1350°C in a ceramic foam filter, using design as in Figure 2. Channel thickness is 4 mm. Dot lines roughly show the liquid front in each frame.

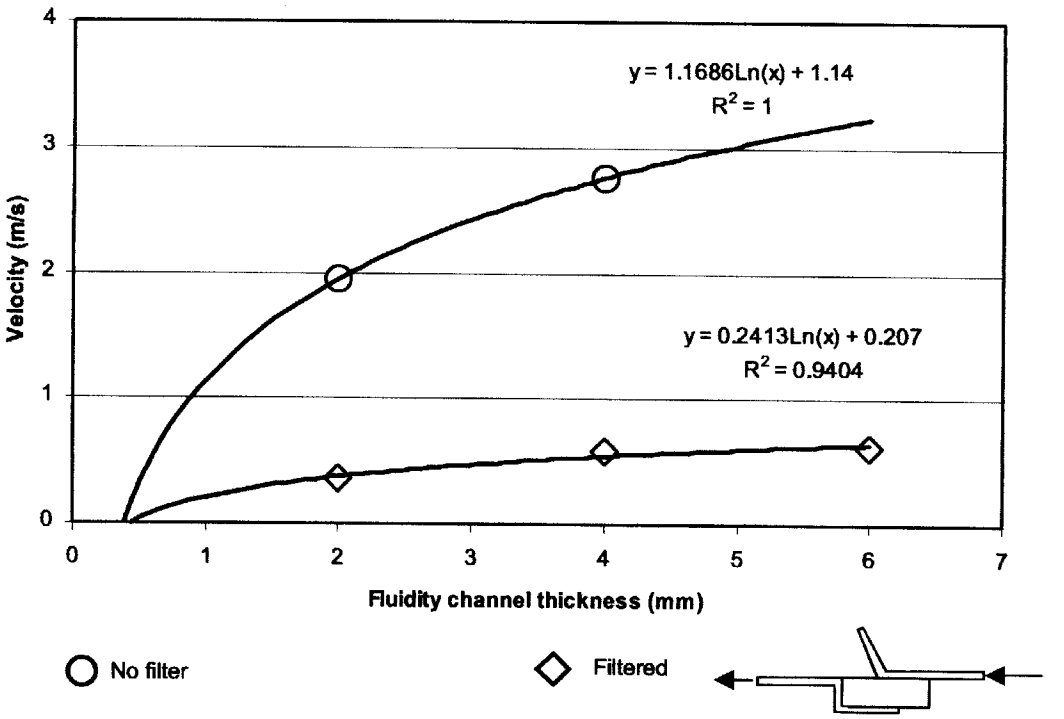

Figure 5: The velocity of liquid Al-%Si alloy at the exit of different filter system and in different thickness of fluidity channels. Data acquired from real time x-ray radiography images.

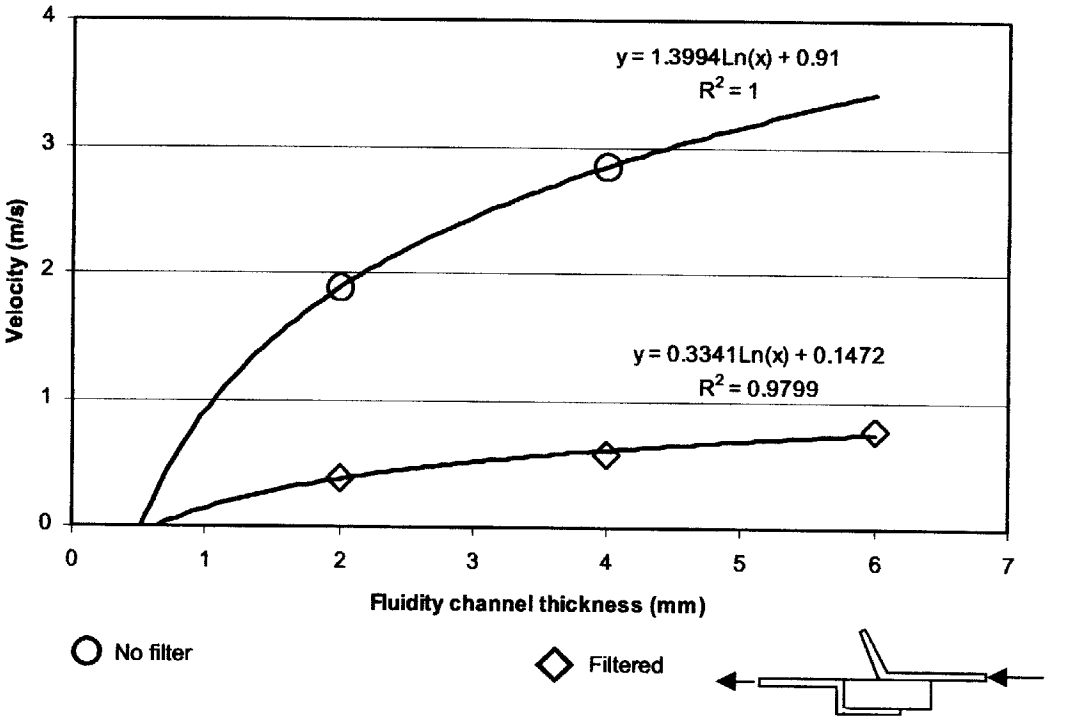

Figure 6: The velocity of liquid cast iron cast at 1350°C at the exit of different filter system and in different thickness of fluidity channels. Data acquired from real time x-ray radiography images.

The flow of liquid Al-Si alloy in a 4 mm thick main channel, recorded by the video x-ray radiography unit is shown in Figure 3. A review of this figure reveals the following series of events (1) the liquid Al-Si alloy flows into the filter inlet; (2) the liquid front enters the bubble trap but the liquid does not fill the trap completely; (3) the trap fills and liquid starts to penetrate the filter. A closely similar sequence is seen for cast iron (Figure 4). The velocities of the liquids with and without a filter in place are presented in Figures 5 and 6 (the zero points on the x axis are assumed from the knowledge that the metal cannot enter a section of about 0.5 mm thickness because of the effect of capillary repulsion).

The simulation results of filling of filter system using the first model (MAGMAsoft package) are shown in Figure 7.

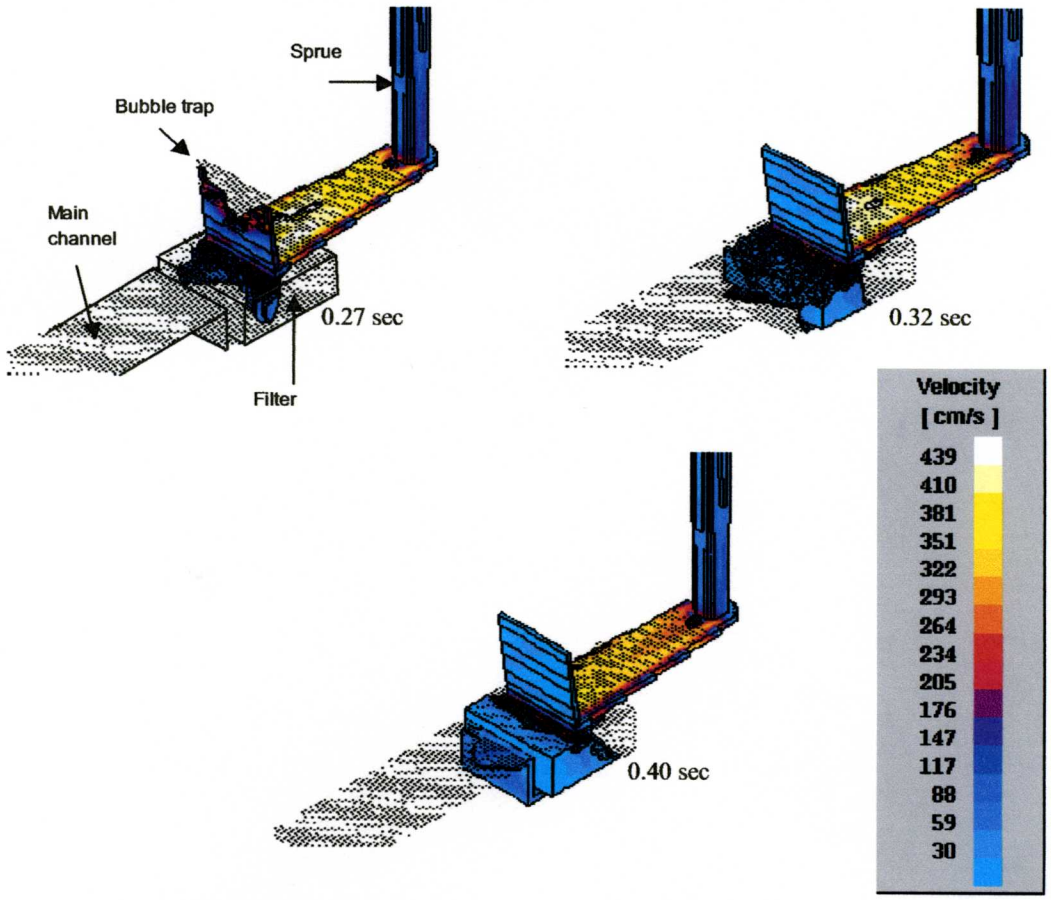

Figure 7: Magmasoft prediction of flow pattern and velocity contours of liquid Al-Si in the D3 filter system.

Figures 8-10 show the simulation results of liquid flow inside of the filter system by the use of second and third models (FLOW3D). Figure 11 illustrates effect of the filter porosity on the velocity of liquid metal in the main channel, using the third filter model.

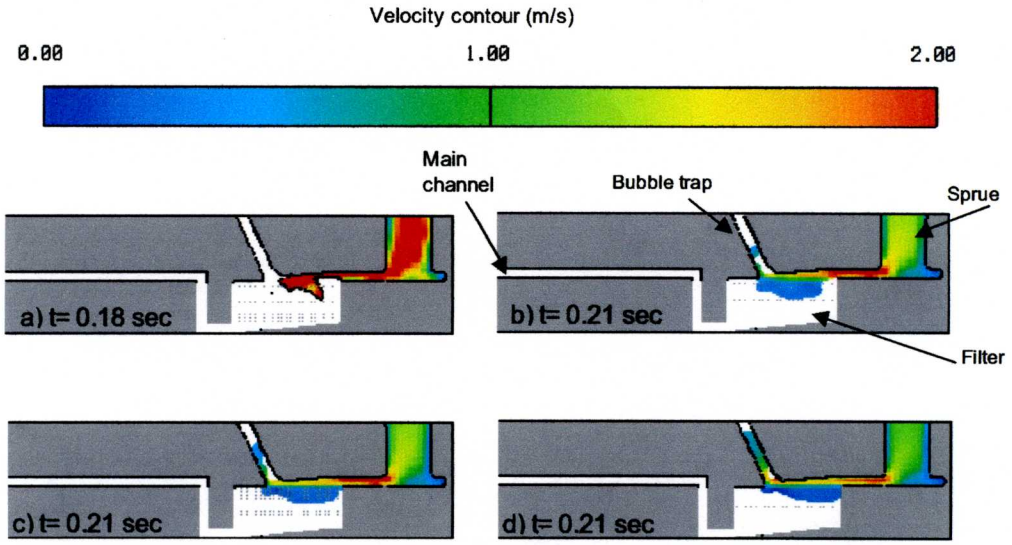

Figure 8: Simulation results of velocity contours when liquid metal enters the filter, in condition of a) Darcian flow and V_F=75%, b, c and d) Inertial dependant flow (second filter model in FLOW3D) with V_F equal to 92, 75 and 55, respectively and the filter surface area per volume is 1000 m^2/m^3 (V_F is porosity percent of filter). Red and blue colours show zero and 2 m/s liquid velocity respectively, and colours between represent velocities up to 2 m/s.

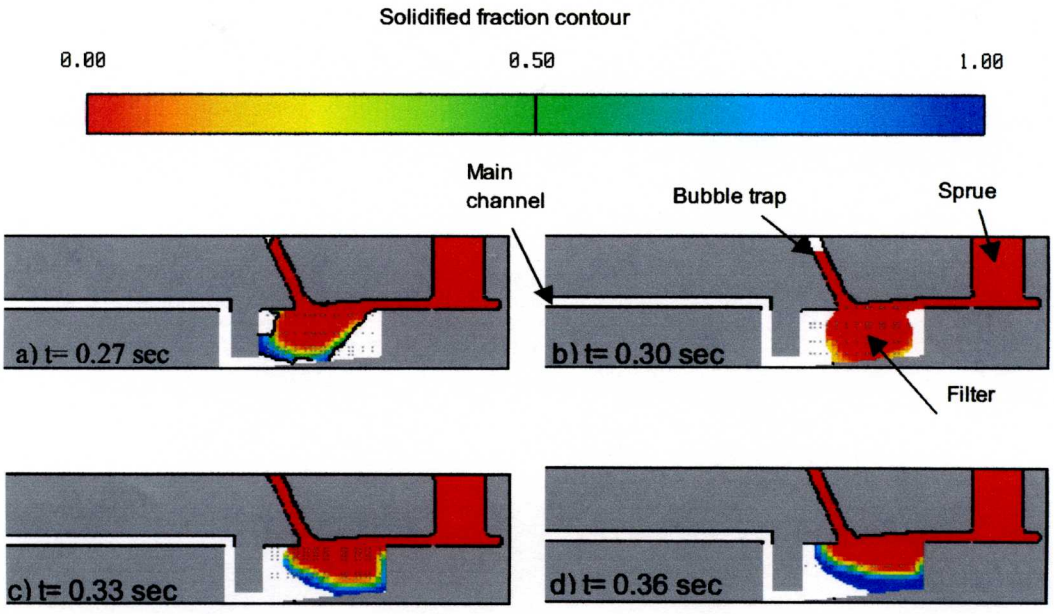

Figure 9: Simulation results of solidified fraction when liquid metal touches the bottom of filter outlet, other conditions as Figure 8. Red and blue colours show zero and 100% solid areas, respectively, and colours between represent mixtures of liquid and different amount of solid.

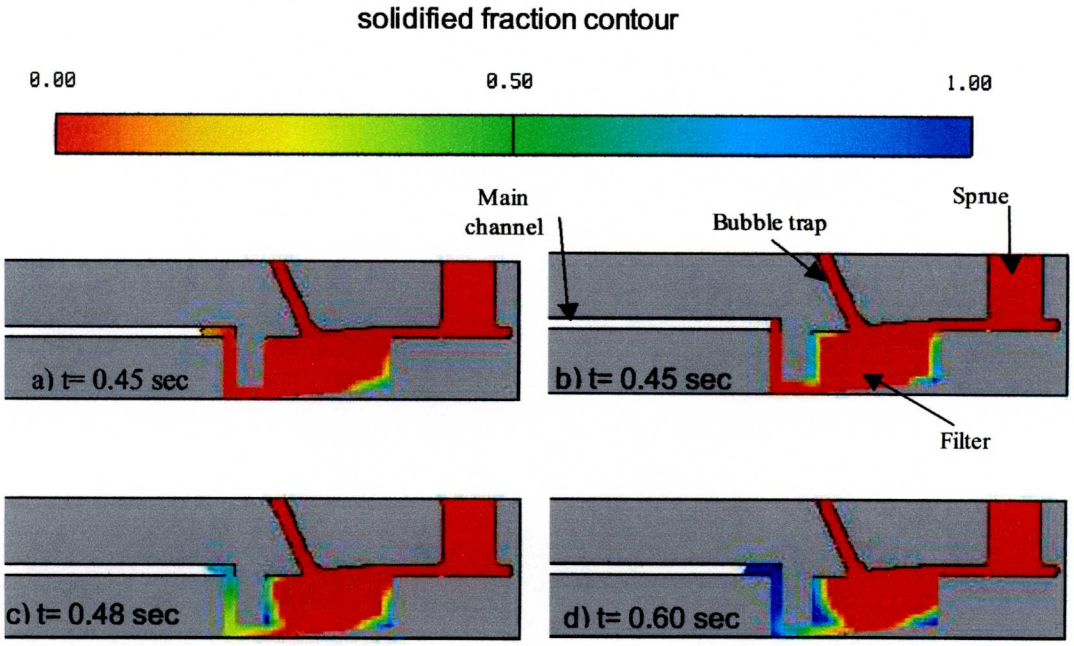

Figure 10: simulation results of solidified fraction when liquid enters the main channel, other conditions as Figure 8. Red and blue colours show zero and 100% solid areas, respectively, and colours between represent mixtures of liquid and different amount of solid.

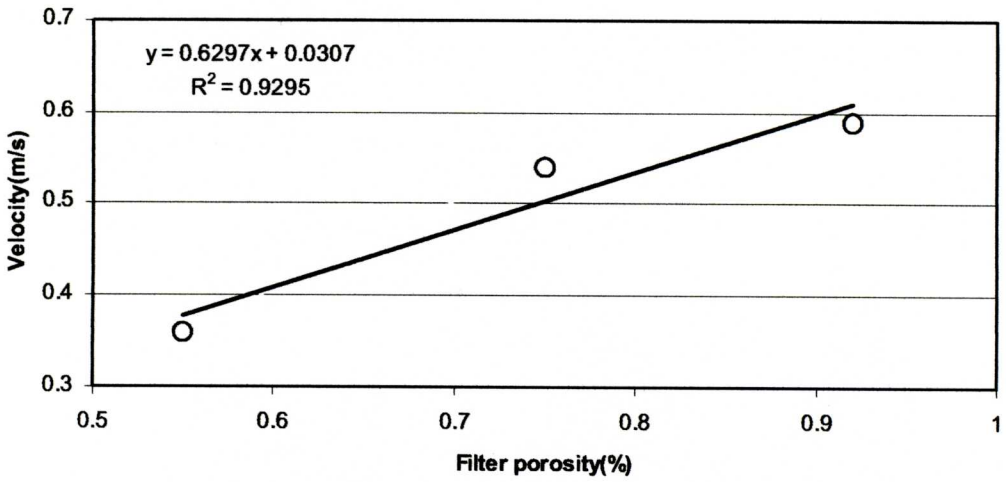

Figure 11: Effect of porosity percent of filter on velocity of liquid Al-%Si in the main channel (after filter system) using second model of the filter in FLOW3D software, the surface area per unit volume of filter is 1000 m^2/m^3.

Comparisons between results of experiments and the simulations for the flow time from top to the bottom of the filter are shown in Figures 12. Comparisons of the velocity of flow of metal entering the main fluidity channel are shown in Figure 13.

	Experiment	Simulation		
		First model	Darcian flow (FLOW3D first model)	Inertial dependant flow (FLOW3D second model)
Time (sec)	0.12	0.08	0.1	0.11

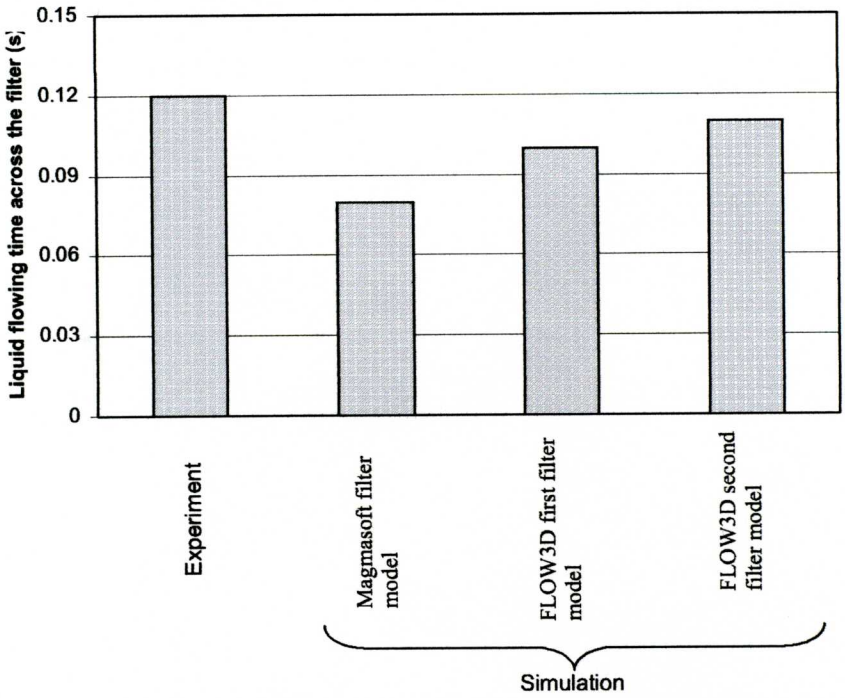

Figure 12: Comparison between Simulation and experimental result of liquid flowing time through the filter.

Figure 14 shows the results of the simulation of the filter system by the second model (assuming inertially dependant flow).

Figure 15 and 16 record the calculated pressure drops from model 3 through the filters for the Al alloy and for cast iron, showing ΔP to increase with the square of the speed of flow.

Liquid velocity without filter(m/s)			Liquid velocity after filter (m/s)			
Experiment	Simulation		Experiment	Simulation		
	MAGMAsoft code	FLOW3D code		MAGMAsoft filter model	Darcian flow* (FLOW3D first filter model)	Inertial dependant flow** (FLOW3D second filter model)
2.85	4.56	2.1	0.58	2.62	0.67	0.59

*Porosity of filter 75% ** Porosity of filter 70%

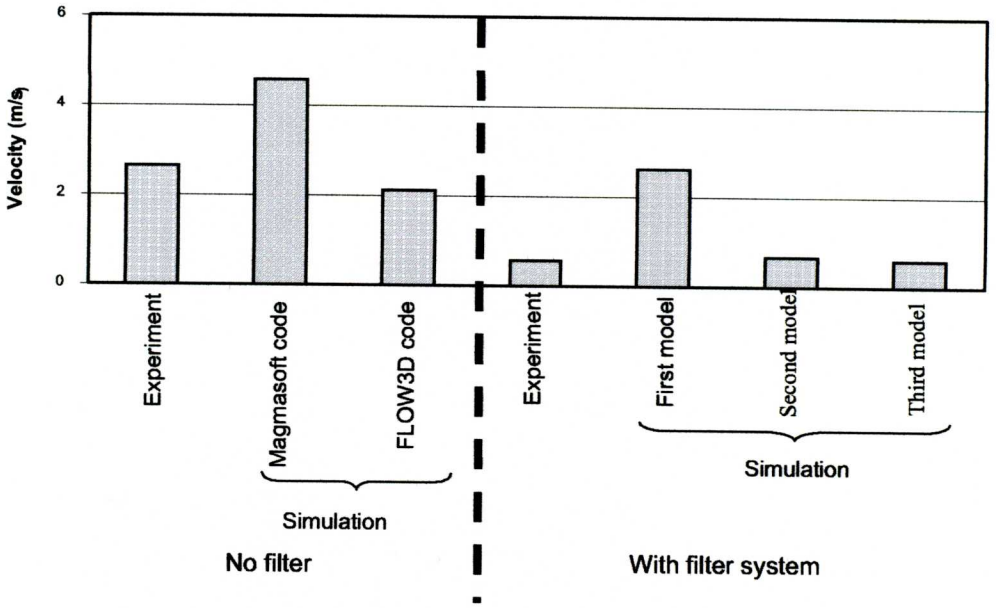

Figure 13: Comparison results of the liquid velocity in the main channel in experiments and simulations.

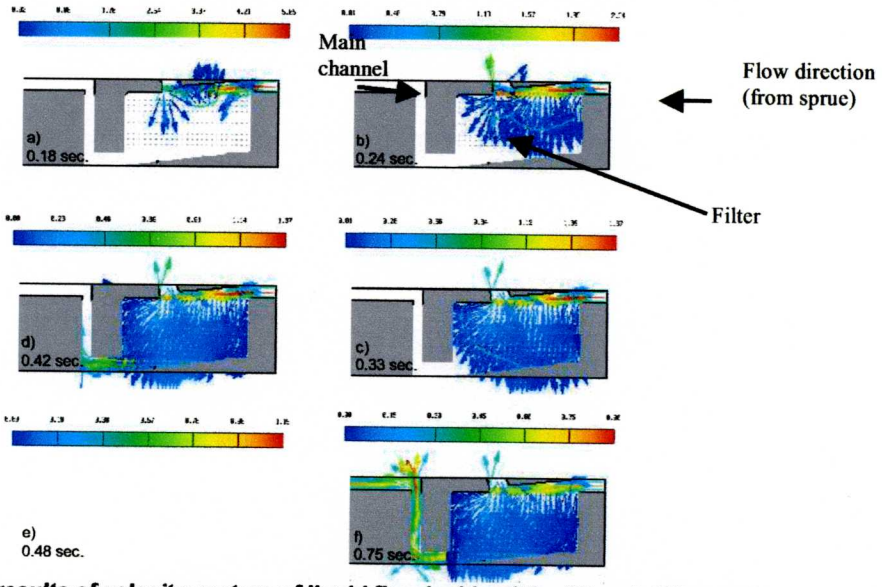

Figure 14: Simulation results of velocity vectors of liquid flow inside of the filter at different times, using the second filter model of FLOW3D software with 92% filtervolume porosity and 10000 m^2/m^3 filter surface area.

Channel thickness (mm)	V_{exit} (m/s)	V_{inlet} (m/s)	V_{inlet}^2 $(m/s)^2$	Pressure drop (MPa)
2.00	0.36	1.95	3.80	4.41
4.00	0.58	2.76	7.62	8.74
6.00	0.62	3.23	10.46	12.10

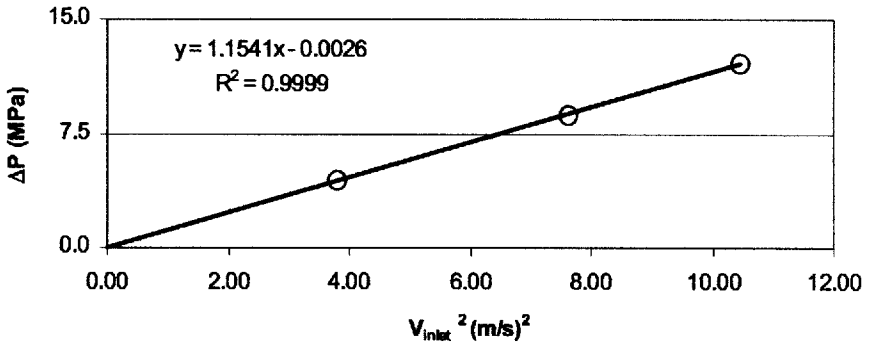

Figure 15: Pressure drop (ΔP) at the filter system versus inlet velocity (to the filter system) of Al-Si alloy melt at 700°C. The inlet velocity for 6 mm thick channel was extrapolated from trend of variation in Figure 5.

Channel thickness (mm)	V_{exit} (m/s)	V_{inlet} (m/s)	V_{inlet}^2 $(m/s)^2$	Pressure drop (MPa)
2.00	0.39	1.88	3.53	11.84
4.00	0.58	2.85	8.12	27.25
6.00	0.77	3.42	11.68	38.82

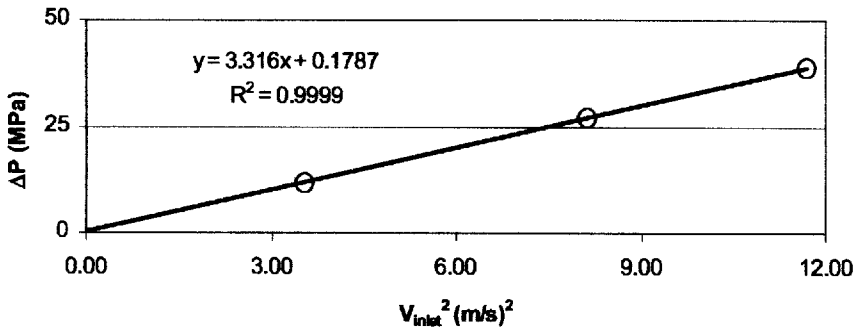

Figure 16: Pressure drop (ΔP) at the D3 filter system versus inlet velocity (to the filter system) of cast iron melt at 1350°C. The inlet velocity for 6 mm thick channel was extrapolated from trend of variation in Figure 6.

DISCUSSION

THE FLOW REGIME IN THE FILTER

When standing back from the simulation results, in general terms all the models are very reasonable approximations to the flow as seen in the x-ray video. Thus, following this accolade, this study concentrates on the finer details of the differences. The differences are revealing in a number of ways as will become clear.

The speed of flow inside the filter can be easily estimated from the measurements in Figure 13. The time for the liquid to pass through the filter is 0.12 s and as the thickness of the filter is 0.02 m, the average velocity V is 0.02/0.12 = 0.167 m/s. Assuming the viscosity of aluminum is approximately 2.5×10^{-3} Pa.s (10), the density of aluminum 2500 kg/m^3, and the average pore diameter of a 20ppi filter is approximately 1 mm, we have Reynold's number

$$R_e = V\, d\rho/\mu \qquad \text{Equation 5}$$
$$= 0.167 \times 10^{-3} \times 2500/0.0025 = 167$$

This number is 2 orders of magnitude less than that required for turbulent flow. It emphasizes the very calm laminar conditions of flow in the filter. Outside the filter, in the entrance to the 4 mm thick fluidity channel, the liquid velocity is 0.58 m/s (Table 1), giving Re (= 0.58 x 0.002 x 2500/0.0025) = 1160. Although this is still less than the critical value of around 20,000 required for turbulent flow, the stability of laminar flow is somewhat less robust than that in the filter.

The simulation results reveal that the shape of the liquid front inside the filter is different for each of the selected filter models. Figure 7 shows, by the use of the first model (assuming turbulent flow), the liquid front flows directly towards the far end of the filter and then turns down. From the Darcy flow model, the liquid front initially flows to the filter instead of the bubble trap (Figure 8a), and fills the bubble trap only at the later stage of the flow (Figures 9a and 10a), which is in contrast with experimental results (Figure 3). It seems that the Darcy flow model is not without its problems.

In view of the strong stability of laminar flow as indicated by Reynolds number, it seems perverse that the computer model based on a component of inertial dependant flow (Model 3) most accurately predicts the liquid metal flow front as seen in the x-ray video (Figures 3 and 10 to 12). This has to pose questions regarding the reliability of the computer model of filters at this time.

The comparison of the measured values in the experiments and simulations, as shown in Figures 12 and 13, again confirm the better agreement of the inertial dependent flow model with the experimental results. The use of 92% porosity for the 20-ppi filter in the simulation (Figures 8b to 10b) is in fairly good agreement with the filling sequence of the filter (Figure 3). However, the apparent accuracy of simulation in this case has to be set against the results of the sensitivity analysis for the effect of porosity on velocity as seen in Figure 11. It is quite clear that the speed of flow can be adjusted up or down by 20 or 30 per cent depending on the choice of porosity. Furthermore, it seems that porosity is not easily measured in practice.

There are likely to be a number of reasons why the flow details predicted by the computer models are not quite accurate.

A potentially important effect neglected by all of the models is the presence of a surface film on the liquid. The film is expected to be an oxide film on the Al alloy, and may be a graphite film on the cast iron. A film represents a challenge for future modellers.

The other noticeable and important point from the simulation studies is the cooling of the advancing flow by the filter media, causing partial solidification near the flow front (Figure 9). This layer of slurry will necessarily restrict the flow of the liquid. However, it is perhaps significant that the computer models do not include this effect, but still, in some cases (eg Model 2) still get a remarkably accurate answer. A close study of velocity vectors in Figure 14 reveals that some of the melt recirculates, travelling upwards through the filter to rejoin the main flow once again. It is this liquid that travels furthest in the filter that is in greatest danger of freezing.

There is, therefore the danger that the liquid could freeze and block the filter at low superheats. The freezing of the liquid is unfortunately well known in the case of ceramic filters of high thermal capacity such as those used for steel. However, in this case, where the continuing flow of liquid has an enough thermal energy, it can remelt this solidified region and open a way through as illustrated in Figure 10.

PRESSURE DROP IN THE FILTER SYSTEM

The pressure drop (ΔP) across the filter can be found from the difference between the kinematic energy of inlet and outlet flows:

$$\Delta P = \tfrac{1}{2} \rho V_{inlet}^2 - \tfrac{1}{2} \rho V_{outlet}^2$$

$$= \tfrac{1}{2} \rho (V_{inlet}^2 - V_{outlet}^2) \qquad \text{Equation 6}$$

The pressure drop in the system can be calculated from measured values in Figures 5 and 6. The use of Equation 6 results in graphs of pressure drop (ΔP) in the filter system versus square of the inlet velocity (Figures 15 and 16). The graphs indicate that a straight line fits the data of both alloys well. It indicates agreement with an inertial dependant flow inside the whole filter system (Equation 4), confirming simulation results. However it is important to note that the pressure drop (ΔP) variations relate to the whole filter system (including the inlet, the filter and the outlet) and not just to the filter media.

From Figures 5 and 6 at a similar velocity the pressure drop for liquid aluminium alloy compared to liquid cast iron is the fraction 1.15/3.32 = 0.346. This is very similar to the ratio of their viscosities 2.5/7.02 = 0.356, almost certainly confirming the importance of the component of laminar viscous flow to overall pressure drop as described by the Darcy equation, in which, of course, the pressure drop is linearly related to the viscosity of the liquid.

It seems likely, therefore, that the strong indication from the size of the Reynold's Number that the flow inside the filter is laminar is in fact correct. The choice of K values in the Magma model was therefore unfortunate and probably contributed to the least accurate result. Even so, it has to be emphasised, that all the simulation results were overall remarkable accurate, illustrating the robustness of the computational techniques currently available. All, however, would benefit greatly from improved input data.

CONCLUSIONS

1. Although the mixed flow model appears to give the most accurate simulation in this study, it has to be concluded that the agreement is probably fortuitous, and influenced by the strong sensitivity of the results to the choice of the density of the filter, which is not easily measured.

2. Thus in the conditions of this study, it seems most likely that the flow regime inside the filter is a laminar, viscosity dependent flow, as described by the Darcy equation. It is just possible that outside the filter an inertially dependent flow may occur. The total effect of the filter system is then probably described well by a mixed flow regime. This would definitely be the case for a normal filter print in which large volumes exist at the entrance and exit of the filter to spread the flow (but unlikely in the present study as a result of the narrow channels used here).

3. The filter causes a pressure drop in the stream from the following major causes:

a) A frictional effect due to viscous Darcy type flow inside the filter.
b) An additional effect due to turbulent drag outside most conventional filters, in the expanded approach and exit. The turbulence effect is not convincingly seen in this work because the approach and exit channels are especially narrow; apparent evidence is probably attributable to inappropriate choice of physical materials data selected for input.
c) A solidification effect that is important during the priming of the filter, especially when the superheat of the liquid is low. At high superheats this effect would be eliminated as the filter heats up. The thickness of the solidified front of the liquid in the filter increases as the porosity of the filter decreases.

ACKNOWLEDGEMENTS

The authors would like to thank Professor I. R. Harris, head of the Institute of Metallurgy and Materials and Professor M. H. Loretto, Director of the IRC in Materials Processing at the University of Birmingham for the provision of research facilities. One of authors (A.H.Zadeh) would like to acknowledge the Ministry of Higher Education of I. R. Iran and Semnan University, Iran, for the sponsorship of his PhD work at the University of Birmingham.

REFERENCES

1. Runyoro J, Boutorabi S. M. A., Campbell J. (1992), Critical gate velocity for film forming casting alloys, AFS Transactions, 37, 225-239.
2. Mutharasan R., Apelian D., Romanowski C. (1981), A laboratory investigation of aluminium filtration through deep-bed and ceramic open-pore filters, J. Metals, 83, (12), 12-18.
3. Mutharasan R., Apelian D., Ali S. (1985), Physical refining of steel melts by filtration, Metallurgical Trans., 16B, 752-7742.
4. Philipse A. P., Schram H. L. (1991), Non-Darcian airflow through ceramic foams, J. Am. Ceramic Soc., 74, (4), 728-732.
5. Lo H. S. H. (1998), Ph.D. thesis, The University of Birmingham, Birmingham UK.
6. Habibollah Zadeh A., Campbell J., Filter systems for high velocity liquid metal flow, To be published.
7. Habibollah Zadeh, A., (2001), Ph.D. thesis, The University of Birmingham, Birmingham, UK.
8. MAGMAsoft Manual version4.0.
9. FLOW3D manual version 7.5.
10. Lage J.L., Anothe B.V., Price D.C., and Weber R.M., Two types of nonlinear pressure-drop versus flow-rate relation observed for saturated porous media, ASME journal of Fluid Engineering, Vol. 119, 1997, p 700-706.
11. Themelis, N. J., (1995), Transport and chemical rate phenomena, Gordon and Breach Publishers.
12. Angus, T., (1976), Cast iron: physical and engineering properties, 2nd edition, Butterworths Publisher.